ELSEVIER

International Journal of Heat and Fluid Flow 22 (2001) 10–18

International Journal of HEAT AND FLUID FLOW

www.elsevier.com/locate/ijhff

Development of a near-wall turbulence model and application to jet impingement heat transfer

Tae Seon Park [a], Hyung Jin Sung [b,*]

[a] *Space Propulsion Department, Rocket Technology Division, Korea Aerospace Research Institute, 52 Oun-dong, Yusong-ku, Taejon 305-333, South Korea*

[b] *Department of Mechanical Engineering, Korea Advanced Institute of Science and Technology, 373-1 Kusong-dong, Yusong-ku, Taejon 305-701, South Korea*

Received 30 March 1998; accepted 4 July 2000

Abstract

A near-wall turbulence model was developed and applied to heat and fluid flows for an impinging jet flow. The k–ε–f_μ model was modified for predictions in strongly strained turbulent flows. To derive a realizable eddy viscosity, the $f_{\mu 2}$ function was newly formulated. The near-wall effect and the anisotropic production were reflected in the ε-equation. The model performance was validated by the relevant experimental data. The predicted results were compared with those by the k–ε model and by the k–ε–v^2 model. The application to jet impingement heat transfer revealed that the present numerical predictions of wall heat transfer show good agreement with the experimental data in the stagnation region. The influence of the Reynolds number on the stagnation Nusselt number was investigated. The model performance was shown to be generally satisfactory.

1. Introduction

Jet impingement heat transfer is used in many engineering and industrial applications. These include cooling of electronic components, drying paper, textiles and tempering of glass. This technique is very attractive and cost-effective because it can increase heat flux significantly near the stagnation point (Behnia et al., 1998). The impinging jet flow, despite its relatively simple geometry, exhibits extremely complex flow characteristics. Among others, the flow in stagnation region is nearly irrotational and there is a large total strain along the streamline. Also, it turns in the radial direction with substantial curvature. Away from this region, the flow forms wall jet boundary layers along the plate. An accurate prediction of flow and attendant heat transfer in the jet impingement poses a significant problem.

Comprehensive knowledge of flow structure is an essential building block to analyze the attendant heat transfer. To predict a jet impingement heat transfer accurately, reliable flow computations with an appropriate turbulence model should be preceded. A literature survey reveals that many turbulence models have been assessed for jet impingement heat transfer. Four turbulence models were tested by Craft et al. (1993a,b) with relevant experimental data (Baughn and Shimizu, 1989; Baughn et al., 1991; Cooper et al., 1993). They employed one k–ε eddy viscosity model and three second moment closure models for turbulence model assessments. Their numerical predictions indicated that the k–ε turbulence model shows a substantial overprediction in the stagnation region of an impinging jet, while some second moment closure models present better predictions near the stagnation region. Behnia et al. (1998) applied the k–ε–v^2 model to jet impingement heat transfer. Their numerical predictions gave much better agreement with experimental data, especially the wall heat transfer in the stagnation region.

Recently, a new k–ε–f_μ model has been developed by Park and Sung (1997). In their model, the near-wall effect without reference to distance and the non-equilibrium effect were incorporated. The non-local near-wall effect was taken into account by an elliptic relaxation approximation for the wall damping function. The local anisotropy in strongly strained turbulent flows was also introduced in the ε-equation. It was shown that the eddy viscosity plays an important role in the prediction of shear flows away from the wall. These model characteristics can improve the predictions of jet impingement flow and heat transfer. In particular, the near-wall heat transfer of strongly strained turbulent flows in the stagnation region is well predicted by the mean strain dependent damping function (Craft et al., 1996).

In the present study, a modified k–ε–f_μ model is developed and applied for predicting an axisymmetric impinging jet flow, where a fully developed turbulent jet is perpendicular to the flat plate with uniform heat flux. The variation of C_μ was achieved with the aid of the Cayley–Hamilton theorem (Park, 1999). The near-wall effect and the anisotropic production

* Corresponding author.
E-mail address: hjsung@kaist.ac.kr (H.J. Sung).

0142-727X/01/$ - see front matter
PII: S0142-727X(00)00069-2

Notation

D	jet diameter
ER	expansion ratio of backward-facing step
h	wall heat transfer coefficient, $h = q_w/(\Theta - \Theta_j)$
H	jet-to-plate distance
H_b	height of backward-facing step
k	turbulent kinetic energy
k_f	thermal conductivity
Nu	Nusselt number, $Nu = hD/k_f$
Pr	Prandtl number
q_w	constant surface heat flux
r	radial distance
Re_D	Reynolds number based on bulk velocity, $Re_D = U_b D/\nu$
U	mean velocity
U_b	jet bulk velocity
X_R	reattachment length
Greeks	
δ_{ij}	Kronecker delta
Θ	mean temperature
Θ_j	jet temperature
ε	dissipation rate of turbulent kinetic energy
κ	von Karman constant

were also reflected in the ε-equation. The model validation was made by comparing the predicted results with those by the k–ε model and the k–ε–v^2 model (Behnia et al., 1998). Profiles of the normalized velocity and distributions of the local wall heat transfer coefficient were analyzed for various Reynolds numbers ($Re_D = 23\,000$, 50 000 and 70 000). The predicted results were compared with the experimental data (Baughn and Shimizu, 1989; Baughn et al., 1991; Cooper et al., 1993; Yan, 1993). The predicted results were shown to be generally satisfactory.

2. Low-Reynolds number k–ε–f_μ model

2.1. Governing equations

For an incompressible turbulent flow, the governing equations are written in Cartesian tensor notation as

$$\frac{\partial U_i}{\partial x_i} = 0, \tag{1}$$

$$U_j \frac{\partial U_i}{\partial x_j} = -\frac{1}{\rho}\frac{\partial P}{\partial x_i} + \frac{\partial}{\partial x_j}\left[\nu \frac{\partial U_i}{\partial x_j} - \overline{u_i u_j}\right], \tag{2}$$

where U_j and u_j are the jth components of the mean and fluctuating velocities, respectively, P the mean pressure, ρ and ν are the fluid density and kinematic viscosity. In the k–ε–f_μ model of Park and Sung (1997), the unknown Reynolds stress $-\overline{u_i u_j}$ can be expressed in a conventional form as

$$-\overline{u_i u_j} = \nu_t\left(\frac{\partial U_i}{\partial x_j} + \frac{\partial U_j}{\partial x_i}\right) - \frac{2}{3}k\delta_{ij} \tag{3}$$

$$\nu_t = C_\mu f_\mu \frac{k^2}{\varepsilon} \tag{4}$$

$$U_j \frac{\partial k}{\partial x_j} = \frac{\partial}{\partial x_j}\left[\left(\nu + \frac{\nu_t}{\sigma_k}\right)\frac{\partial k}{\partial x_j}\right] + P_k - \varepsilon \tag{5}$$

$$U_j \frac{\partial \varepsilon}{\partial x_j} = \frac{\partial}{\partial x_j}\left[\left(\nu + \frac{\nu_t}{\sigma_\varepsilon}\right)\frac{\partial \varepsilon}{\partial x_j}\right] + P_\varepsilon^1 + P_\varepsilon^2 + P_\varepsilon^3 + P_\varepsilon^4 - \Gamma. \tag{6}$$

In the above equations, C_μ, σ_k and σ_ε are the model constants. The production of turbulent energy P_k is defined as $P_k \equiv -\overline{u_i u_j}\partial U_i/\partial x_j$. The damping function f_μ is obtained by solving the elliptic f_w equation, which introduces the effects of wall-proximity and non-equilibrium away from the wall. In the ε-equation, P_ε^1, P_ε^2, P_ε^3, P_ε^4 and Γ represent the mixed production, production by mean velocity gradient, gradient production, turbulent production and destruction in sequence, respectively (Park and Sung, 1997). The variations of C_μ in the eddy viscosity ν_t are allowed by decomposing f_μ into two parts, i.e., $f_\mu = f_{\mu 1} f_{\mu 2}$, where $f_{\mu 1}$ signifies the effect of wall proximity in the near-wall region while $f_{\mu 2}$ represents the effect of non-equilibrium away from the wall (Park and Sung, 1995).

The wall-proximity function $f_{\mu 1}$ is obtained by solving an elliptic relaxation equation for the wall damping function (f_w):

$$\nu_t = C_\mu f_{\mu 1} f_{\mu 2} \frac{k^2}{\varepsilon}, \tag{7}$$

$$f_{\mu 1} = \left(1 + C_{W1}\ \exp[-(R_t/C_{W2})^2]R_t^{-3/4}\right) f_w^2, \tag{8}$$

$$\frac{\partial^2 f_w}{\partial x_j \partial x_j} = \frac{R_t}{A^2 L^2}(f_w - 1). \tag{9}$$

Here, C_{W1}, C_{W2} and A are the model constants and L is a turbulence length scale. The turbulent Reynolds number R_t is defined as $R_t \equiv k^2/\nu\varepsilon$. Note that the argument of Eq. (9) is very similar to the conception of Durbin (1993, 1996). However, its physical meaning is different. Details regarding the derivation of f_w equation can be found in Park and Sung (1997).

As the wall is approached, R_t decreases rapidly and L is reduced. The energy-containing and energy-dissipating eddies have nearly the same order of magnitude in the vicinity of the wall so that the influences of low turbulence Reynolds number and viscosity are strong. To account for these effects, a length scale related to the damping function should be modeled. A turbulence length scale L is adopted as (Durbin and Laurence, 1996)

$$L = \sqrt{\frac{k^3}{\varepsilon^2} + C_L^2\left(\frac{\nu^3}{\varepsilon}\right)^{1/2}}, \tag{10}$$

where the viscous layer close to the wall is represented by the Kolmogorov small eddies, while the region away from the wall is represented by the energy-containing eddies. Since A and L in Eq. (9) represent the influence of wall proximity, the larger value of A and L enhances the effect of wall damping and it yields a thick viscous sublayer. The model constants are set: $C_\mu = 0.09$; $C_{W1} = 15$; $C_{W2} = 120$; $A = 2.4$; $C_L = 70$ (Durbin and Laurence, 1996; Park, 1999).

Next, the $f_{\mu 2}$ function is newly formulated, which describes the variation of C_μ away from the wall. The derivation of $f_{\mu 2}$ starts from the Reynolds stress ($\tau_{ij} = \overline{u_i u_j}$) transport equation in a homogeneous flow,

$$\frac{D\tau_{ij}}{Dt} = -\tau_{ik}\frac{\partial U_j}{\partial x_k} - \tau_{jk}\frac{\partial U_i}{\partial x_k} + \Phi_{ij} - \varepsilon_{ij}, \tag{11}$$

where Φ_{ij} and ε_{ij} denote the pressure–strain correlation and the dissipation rate tensor, respectively. In a local equilibrium state, $Db_{ij}/Dt = 0$ where b_{ij} is the anisotropy tensor $b_{ij} = \tau_{ij}/(2k) - \delta_{ij}/3$. A general algebraic form of b_{ij} is obtained by employing the model of Speziale et al. (1991) and the Kolmogorov assumption $\varepsilon_{ij} = 2\varepsilon\delta_{ij}/3$,

$$b_{ij}2g = \left(C_3 - \frac{4}{3}\right)S^*_{ij} + (C_4 - 2)\left(b_{ik}S^*_{jk} + b_{jk}S^*_{ik} - \frac{2}{3}b_{mn}S_{mn}\delta_{ij}\right) + (C_5 - 2)\left(b_{ik}W^*_{jk} + b_{jk}W^*_{ik}\right), \quad (12)$$

where $S^*_{ij} = 0.5(U_{i,j} + U_{j,i})k/\varepsilon$, $W^*_{ij} = 0.5(U_{i,j} - U_{j,i})k/\varepsilon$ and $g = C_1/2 + P_k/\varepsilon - 1$, respectively. The model constants C_1 and C_3–C_5 are employed from the pressure–strain model of Speziale et al. (1991).

In a matrix form, Eq. (12) can be written as

$$\mathbf{b} = \alpha_1\mathbf{S} + \alpha_2\left(\mathbf{bS} + \mathbf{Sb} - \frac{2}{3}\{\mathbf{bS}\}\mathbf{I}\right) + \alpha_3(\mathbf{Wb} - \mathbf{bW}), \quad (13)$$

where the model constants are summarized as: $\alpha_1 = (C_3 - 4/3)/2g$; $\alpha_2 = (C_4 - 2)/2g$; $\alpha_3 = (C_5 - 2)/2g$. $\{.\}$ denotes the trace and $\mathbf{I}$ is the identity vector. For a two-dimensional flow, an explicit expression of $\mathbf{b}$ is available in linearly independent tensors that may be formed with $\mathbf{S}$ and $\mathbf{W}$ (Gatski and Speziale, 1993). The general form of algebraic solution is

$$\mathbf{b} = \beta_1\mathbf{S} + \beta_2\left(\mathbf{S}^2 - \frac{1}{3}\{\mathbf{S}^2\}\mathbf{I}\right) + \beta_3(\mathbf{SW} - \mathbf{WS}). \quad (14)$$

To determine the coefficients β_1–β_3, the substitution of Eq. (14) into Eq. (13) gives

$$\begin{aligned}\mathbf{b} = {} & \alpha_1\mathbf{S} + 2\alpha_2\beta_1\left(\mathbf{S}^2 - \frac{1}{3}\{\mathbf{S}^2\}\mathbf{I}\right) + \alpha_3\beta_1(\mathbf{WS} - \mathbf{SW}) \\ & + 2\alpha_2\beta_2\left(\mathbf{S}^3 - \frac{1}{3}\{\mathbf{S}^2\}\mathbf{IS} - \frac{1}{3}\{\mathbf{S}^3\}\mathbf{I}\right) \\ & + (\alpha_3\beta_2 - \alpha_2\beta_3)\left(\mathbf{WS}^2 - \mathbf{S}^2\mathbf{W}\right) \\ & + \alpha_3\beta_3\left(2\mathbf{WSW} - \mathbf{W}^2\mathbf{S} - \mathbf{SW}^2\right). \end{aligned} \quad (15)$$

All higher-order tensor combinations can be reduced with the aid of the Cayley–Hamilton theorem and the following relations:

$$\mathbf{S}^3 = (1/3)\{\mathbf{S}^3\}\mathbf{I} + (1/2)\{\mathbf{S}^2\}\mathbf{IS},$$
$$\mathbf{WS}^2 - \mathbf{S}^2\mathbf{W} = 0,$$
$$\mathbf{WSW} - \mathbf{W}^2\mathbf{S} - \mathbf{SW}^2 = -(1/2)\{\mathbf{W}^2\}\mathbf{IS} - \{\mathbf{W}^2\}\mathbf{IS}.$$

$$\tau_{ij} = \frac{2}{3}k\delta_{ij} - 2k\beta_1 S^*_{ij} + 2k\left[\beta_2\left(S^*_{ik}S^*_{kj} - \frac{1}{3}S^*_{mn}S^*_{mn}\delta_{ij}\right) + \beta_3\left(W^*_{ik}S^*_{kj} - S^*_{ik}W^*_{kj}\right)\right], \quad (16)$$

$$\beta_1 = \frac{-\alpha_1}{1 - \frac{2}{3}\alpha_2^2 S^*_{mn}S^*_{mn} + 2\alpha_3^2 W^*_{mn}W^*_{mn}}, \quad (17)$$

$$\beta_2 = 2\alpha_2\beta_1, \quad (18)$$

$$\beta_3 = \alpha_3\beta_1. \quad (19)$$

A final linear model for τ_{ij} is

$$\tau_{ij} = \frac{2}{3}k\delta_{ij} - 2C^*_\mu\frac{k^2}{\varepsilon}S_{ij}, \quad (20)$$

$$C^*_\mu = \frac{-\alpha_1}{1 - \frac{2}{3}\alpha_2^2 S^*_{mn}S^*_{mn} + 2\alpha_3^2 W^*_{mn}W^*_{mn}}. \quad (21)$$

This is an isotropic eddy viscosity model with the coefficient C^*_μ, which is a function of $S^* = \sqrt{2S^*_{ij}S^*_{ij}}$ and $W^* = \sqrt{2W^*_{ij}W^*_{ij}}$. Recall that C^*_μ returns to 0.09 in the standard k–ε model. The damping function $f_{\mu 2}$ is obtained by $f_{\mu 2} = C^*_\mu/C_\mu$.

Although Eq. (21) provides an excellent description of the near-equilibrium turbulent flows (Gatski and Speziale, 1993), a singularity arises in the case of large S^* and W^*. In the short-time rapid distortion theory, as $S^* \to \infty$, k/k_o retains a value of order one, where k_o is an initial turbulent kinetic energy. Accordingly, $f_{\mu 2}$ shows the following asymptotic behavior, i.e., $f_{\mu 2} \sim 1/S^*$. However, the behavior of C^*_μ demonstrates $C^*_\mu \sim (1/S^*)^2$ as $S^* \to \infty$ and $W^* \to \infty$ in a homogeneous shear flow (Park, 1999).

For a weakly strained turbulent flow, the $f_{\mu 2}$ function of Eq. (21) is rewritten by a Pade approximation,

$$f_{\mu 2} \sim \frac{3\alpha^*_1 g(g^2 + 0.5\alpha^{*2}_2 S^{*2})}{3g^4 + 0.5\alpha^{*2}_2 S^{*2}g^2 + 3\alpha^{*2}_3 W^{*2}(g^2 + 0.5\alpha^{*2}_2 S^{*2})}. \quad (22)$$

Here, the model constants have the following relations:

$$\alpha^*_1 = \alpha_1 g, \quad \alpha^*_2 = \alpha_2 g, \quad \alpha^*_3 = \alpha_3 g.$$

The above relations show the limiting behaviors, $f_{\mu 2} \sim O(1)$ and $g \sim O(1)$ for weak and $f_{\mu 2} \sim 1/S^*$ and $g \sim S^*$ for strong strains. It is seen that Eq. (22) shows a consistent limiting behavior for large and small strain rates.

In an effort to make a realizable linear model for τ_{ij}, the conditions of the non-negativity of normal stresses and the Schwarz's inequality between any fluctuating quantities are imposed. This is a basic physical and mathematical principle that prevents a turbulence model from producing non-physical results. In a limiting flow with the generalized mean strain tensor: $S_{11} = \gamma, S_{22} = -\gamma(1 + \mathbf{a})/2$, $S_{33} = -\gamma(1 - \mathbf{a})/2$ and $S_{ij} = 0$ for $i \neq j$, where $\mathbf{a}$ represents types of flow deformation; axisymmetric contraction ($\mathbf{a} = 0$), plane strain ($\mathbf{a} = 1$) and axisymmetric expansion ($\mathbf{a} = 3$). With this constraint, $f_{\mu 2}$ has the following realizable range, i.e., $0 \leqslant f_{\mu 2} \leqslant 2/(3C_\mu S^*) = 1/(3C_\mu\gamma\sqrt{3 + \mathbf{a}^2}k/\varepsilon)$. A simple function can be derived by the correction of leading term,

$$f_{\mu 2} = \frac{C_{\mu 1} + C_{\mu 2}\xi + (g^2 + \eta^2)(C_\mu g + C_{\mu 3}\xi^2)}{C_{\mu 3}g^4 + C_{\mu 4}(g\eta)^2 + C_{\mu 3}\xi^2(g^2 + \eta^2 + C_{\mu 5}\eta^3)}, \quad (23)$$

where $\eta = C_\mu f_w\sqrt{2S^*_{ij}S^*_{ij}}$, $\xi = 2C_\mu f_w\sqrt{2W^*_{ij}W^*_{ij}}$ and $g = 1 + 0.2\eta$, respectively. The introduction of f_w is that the wall-proximity effect in the near-wall region is significant compared to the strain rate effect. The model constants are determined from the experimental data of Tavoularis and Karnik (1989): $C_{\mu 1} = 7$; $C_{\mu 2} = 4$; $C_{\mu 3} = 6$; $C_{\mu 4} = 13$; $C_{\mu 5} = 10$.

To look into the performance of the model, the behaviors of $-2b_{12} = C_\mu f_\mu S^*$ and $-2b_{11} = C_\mu f_\mu S^*$ are plotted in Fig. 1 for a homogeneous shear flow and an irrotational flow, respectively. A global dependency of turbulent shear stress on S^* is clearly displayed. The results are compared with the experiment of Tavoularis and Karnik (1989). Three models are selected: the models of Craft et al. (1993a,b), Gatski and Speziale (1993) and Cotton and Ismael (1993). Three models show a good prediction for a homogeneous shear flow. However, the model of Cotton and Ismael shows a negative value in highly strained flows. A correct asymptotic behavior is predicted by the present model, which is $f_{\mu 2} \sim 1/S^*$ for $S^* \to \infty$. However, the limiting behaviors of other models are less satisfactory. It is interesting to find that the model of Gatski and Speziale predicts well in a homogeneous shear flow while a non-physical prediction is exhibited in Fig. 1(b). This is attributed to the violation of realizability in an irrotational flow.

2.2. Modeling of the ε-equation

By the scaling argument, P^1_ε, P^2_ε, P^4_ε and Γ terms in Eq. (6) can be modeled in a way similar to the prior models (Park and Sung, 1997)

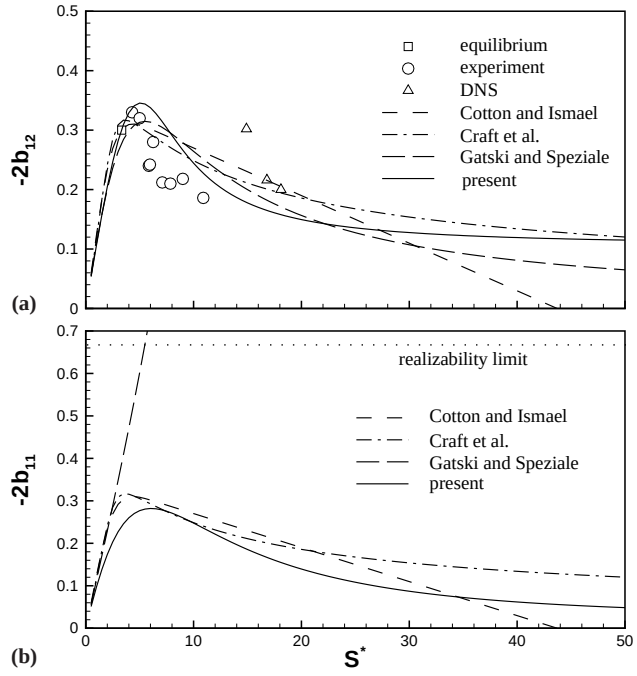

Fig. 1. Comparison of b_{12} and b_{11}. (a) Homogeneous flow; (b) irrotational flow.

$$P_\varepsilon^1 + P_\varepsilon^2 + P_\varepsilon^4 - \Gamma = \left(C_{\varepsilon 1}^* P_k - C_{\varepsilon 2} f_2 \varepsilon\right)/T + C_P(1-f_w)\nu\nu_t\left(\frac{\partial^2 U_i}{\partial x_j \partial x_j}\right)^2, \quad (24)$$

where $C_{\varepsilon 1}^*$, $C_{\varepsilon 2}$ and C_P are the model constants. The turbulent timescale is defined as

$$T = \sqrt{(k/\varepsilon)^2 + C_T^2 T_K^2},$$

where the Kolmogorov timescale is $T_K = \sqrt{\nu/\varepsilon}$ as a lower bound (Durbin and Laurence, 1996). The model constants are $C_T = 6.0$ and $C_P = 0.8$. The model function f_2 in Eq. (24) is expressed as $f_2 = 1 - (2/9)\exp(-0.33R_t^{1/2})$, which describes the effect of decaying turbulence.

Although most prior models have used a constant value $C_{\varepsilon 1}^*$, the variation of $C_{\varepsilon 1}^*$ is sensitive to the non-equilibrium effect (P_k/ε) and to the shear layer spreading rate (Durbin, 1993; Park and Sung, 1995). It is found that $C_{\varepsilon 1}^*$ gives a significant influence on the reattachment length prediction in flows over a backward-facing step (Park and Sung, 1997). This may be attributed to the additional production of dissipation rate by local anisotropy. Speziale and Gatski (1997) also developed $C_{\varepsilon 1}^*$ based on the explicit ε_{ij} relation with S_{ij}^* and W_{ij}^*. Since their model was calibrated for a homogeneous shear flow, the flow prediction in the near-wall region is less satisfactory. In order to incorporate the effect of normal strain rates, a new $C_{\varepsilon 1}^*$ is derived in the present study. Based on the production terms in the ε-equation with the Rotta model,

$$P_\varepsilon^1 + P_\varepsilon^2 = C_{\varepsilon 1}^* P_k \frac{\varepsilon}{k} = -2\nu\overline{\frac{\partial u_i}{\partial x_k}\frac{\partial u_j}{\partial x_k}} S_{ij} = -C_{\varepsilon 1}\frac{\overline{u_i u_j}}{k}\varepsilon S_{ij} = -C_{\varepsilon 1} 2 b_{ij}\varepsilon S_{ij}, \quad (25)$$

$C_{\varepsilon 1}^*$ is obtained by substituting the full anisotropy tensor (Eq. (14)) and the continuity:

$$C_{\varepsilon 1}^* = C_{\varepsilon 1} - C_\mu f_w \frac{\varepsilon}{P_k}\left[\beta_2^*\left(S_{ik}^* S_{kj}^* - S_{mn}^* S_{mn}^* \frac{\delta_{ij}}{3}\right) + \beta_3^*\left(W_{ik}^* S_{kj}^* - S_{ik}^* W_{kj}^*\right)\right] S_{ij}^*, \quad (26)$$

where

$$\beta_2^* = \frac{2 + \xi_*^2(1+\eta_*) + \xi_*^2}{4 + \xi_*^2(1 + 8\eta_*^3) + 35\eta_*^2},$$

$$\beta_3^* = \frac{4 + \xi_*^2(1+\eta_*) + \eta_*^2}{4 + \xi_*^2(1 + 12\eta_*^3) + 40\eta_*^2},$$

$$\eta_* = C_\mu\sqrt{2S_{ij}^* S_{ij}^*}$$

and

$$\xi_* = 2C_\mu\sqrt{2W_{ij}^* W_{ij}^*}.$$

The model constants are determined by using the algebraic equations of β_2^* and β_3^* obtained from the experimental results and numerical optimization for a fully developed channel flow (see Fig. 2). This accounts for the additional production of dissipation by local anisotropy.

The turbulent diffusion terms of k and ε, in general, are modeled by a gradient diffusion type. The values of σ_k and σ_ε are usually taken to be $1.0 \leqslant \sigma_k, \sigma_\varepsilon \leqslant 1.4$. The model constants employed are $\sigma_k = 1.1$, $\sigma_\varepsilon = 1.3$, $C_{\varepsilon 1} = 1.5$ and $C_{\varepsilon 2} = 1.9$.

2.3. Modeling of the temperature equation

In predicting turbulent heat transfer, the modeling of turbulent heat flux based on the Boussinesq approximation is generally used. The unknown eddy diffusivity of heat is

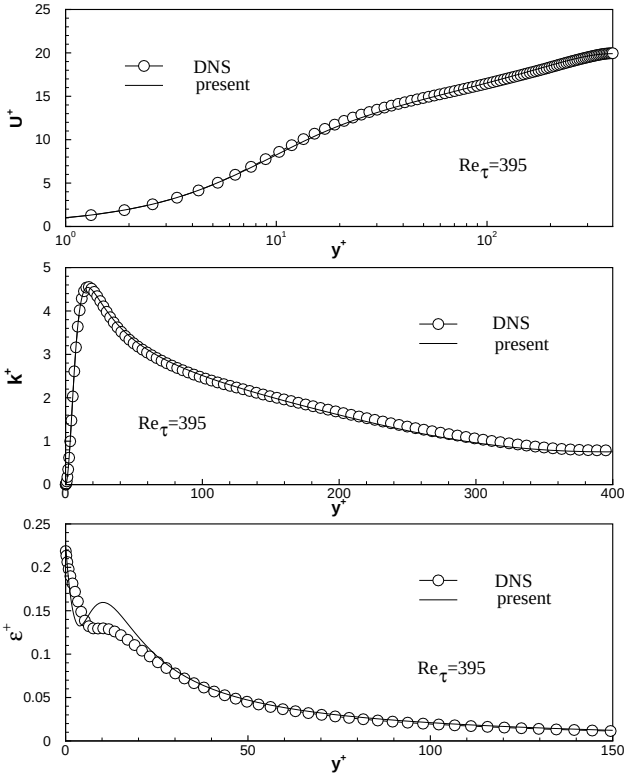

Fig. 2. Comparison of the predicted U^+, k^+ and ε^+.

calculated by prescribing a constant turbulent Prandtl number Pr_t. The governing equation of mean temperature can be expressed as

$$U_j \frac{\partial \Theta}{\partial x_j} = \frac{\partial}{\partial x_j}\left[\left(\frac{\nu}{Pr} + \frac{\nu_t}{Pr_t}\right)\frac{\partial \Theta}{\partial x_j}\right]. \tag{27}$$

The assumption, i.e., $Pr_t = constant$ satisfies Pope's linear principle of scalars in turbulent flows. However, it is revealed that there are no universal values of Pr_t, even in simple wall shear flows. The direct numerical simulation data showed that Pr_t increases towards a wall instead of being constant (Kasagi et al., 1992). Its value is 1.1 at the wall and 0.7–0.9 in the outer region.

Many attempts have been made to get a reliable Pr_t formula which improves the prediction of turbulent heat transfer. A formula, incorporated with a simple conduction model which fits the available experimental data reasonably well for a boundary layer without pressure gradient, has a form as follows (Kays and Crawford, 1993):

$$Pr_t = \frac{1}{0.5882 + 0.228(\nu_t/\nu) - 0.0441(\nu_t/\nu)^2[1 - \exp(\frac{-5.165}{\nu_t/\nu})]}. \tag{28}$$

This yields a value of 1.7 at the wall and an asymptotic value of 0.85 far from the wall. The present model is tested for the effect of Pr_t on the local Nusselt number for impinging jet flows.

2.4. Boundary conditions

A schematic diagram of the jet impingement is shown in Fig. 3. At the jet discharge, the flow is fully developed and isothermal. The inlet condition is obtained by the preceding computation of fully developed pipe flow. The upper computational domain is shown in Fig. 3, which is higher 3–4 times of the jet diameter. This allows the upper boundary to be a sufficient distance from the wall so that it does not affect the flow near the impingement surface. Over the remainder of the upper boundary, an entrainment condition is applied to all variables: properties of the entering fluid satisfy the zero-gradient condition except the radial velocity $U = 0$. At the right-hand outflow boundary, the normal velocities to the boundary are obtained from the continuity and the Neumann condition is applied to all variables. It is found that the right boundary location should be larger than $(8D + H)$ to avoid the flow distortion. The boundary at the left-hand side is a symmetric axis.

Finally, a uniform constant heat flux is applied to the wall to compare the predicted results with the experiments (Baughn and Shimizu, 1989; Baughn et al., 1991; Yan, 1993). A comparison of the condition of constant wall temperature with that of constant heat flux reveals that a little different trend of local

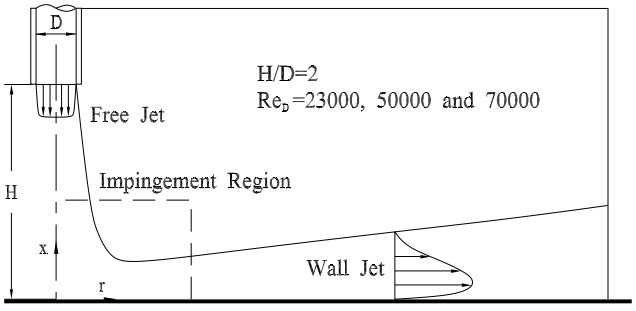

Fig. 3. Flow configuration and computational domain.

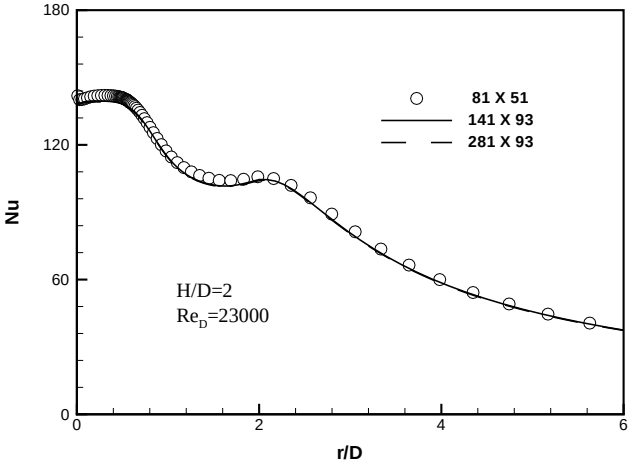

Fig. 4. Grid convergence test.

heat transfer is exhibited. The radial and normal velocity components are set to be zero. The asymptotic behavior $\varepsilon_w \to 2\nu k/n^2$ as $n \to 0$ is applied for all wall boundaries, where n denotes the wall normal direction.

2.5. Numerical procedure

The finite-difference equations were discretized using the hybrid linear and parabolic approximation (HLPA) scheme with second-order accuracy. A non-staggered variable arrangement was adopted with the momentum interpolation technique to avoid the pressure–velocity decoupling. The coupling between pressure and velocity was achieved by the SIMPLEC algorithm. The convergence was accelerated with a multigrid method (Park, 1999). Non-uniform, orthogonal and axisymmetric grid was used with a high resolution near all solid boundaries. The grid convergence was checked by three cases: 81×51, 141×93 and 281×93. The outcome with a 141×93 mesh was found to be satisfactory, as shown in Fig. 4. Two values of the pipe wall thickness were examined, i.e., $0.112D$ and $0.0313D$, which were selected from the experiments of Cooper et al. (1993) and Baughn and Shimizu (1989), respectively. The thickness $0.0313D$ was used for the present computation. The computations were implemented on a CRAY-YMP supercomputer, and a typical CPU time was approximately 0.8 h for a 141×93 mesh. Convergence was declared when the maximum normalized sum of absolute residual source over all the computational nodes was less than 10^{-4}.

3. Results and discussion

3.1. Application to fully developed channel flow

Before proceeding further, it is important to ascertain the generality and accuracy of the present model. The model is tested for a fully developed channel flow for which turbulence quantities are available from the DNS data (Moser et al., 1999). The selected Reynolds number is $Re_\tau = 395$. The profiles of mean velocity, turbulent kinetic energy and its dissipation rate are displayed in Fig. 2. The results of the present model are in good agreement with the DNS data.

In order to assess the model performance of separated and reattaching flows, a flow over a backward-facing step is selected. This flow is frequently used for benchmarking the

Table 1
Comparison of X_R with experiments

Case	ER	Re_{H_b}	Grid	X_R/H_b (Exp.)	X_R/H_b
Driver and Seegmiller	1.125	38 000	233 × 201	6.21 ± 0.2	6.31
Adams et al.	1.25	26 000	233 × 181	6.67 ± 0.3	6.46
Kim et al.	1.50	46 000	233 × 141	7.60 ± 0.3	7.58
Eaton and Johnston	1.667	38 000	233 × 101	7.95 ± 0.3	7.97

performance of turbulence models (Park and Sung, 1997). Table 1 lists the computational conditions and the calculated reattachment lengths X_R/H_b. The present model's results are in excellent agreement with the experiments in the range $1.125 \leqslant \mathrm{ER} \leqslant 1.667$. Here, ER denotes the expansion ratio.

3.2. Realizability

It has been a significant problem of two-equation turbulence models to predict an enormously large growth of turbulent kinetic energy at a stagnation point. Their poor prediction arises from the use of the explicit algebraic stress equation based on S^* and W^*. In a two-dimension flow, the turbulent production due to the irrotational strains is defined as

$$P_k = -\overline{u^2}\frac{\partial U}{\partial x} - \overline{v^2}\frac{\partial V}{\partial y} = 2\nu_t\left[\left(\frac{\partial U}{\partial x}\right)^2 + \left(\frac{\partial V}{\partial y}\right)^2\right]. \tag{29}$$

In the case of stagnation flow, the experimental result indicates $P_k \sim 0$. This is due to the fact that the intensities of normal stresses are nearly the same and $\partial U/\partial x = -\partial V/\partial y$ form the continuity. However, as can be seen in Eq. (29), the production gives a quadratic variation in strain rates. This leads to a spurious generation of turbulent kinetic energy.

In the k–ε model, this anomaly should be prevented by deriving a realizable eddy viscosity. There are several solvable approaches; the first is to introduce a physical time scale or a length scale with the realizability constraint. Durbin (1996) imposed a bound on the time scale in the k–ε–v^2 model. The results of jet impingement heat transfer showed that the stagnation anomaly can be ameliorated by this constraint. The second is to allow the variation of C_μ, which is defined in Eq. (4). The value of $C_\mu = 0.09$ was chosen on the basis of experiments in a local equilibrium flow. However, if the non-equilibrium effect is dominant, C_μ varies depending on the flow conditions.

The deviation from a local equilibrium is expected in the presence of mean deformation of turbulence fields. This is because the energy-containing eddies are strained primarily by the mean deformation. Following Hunt's (1992) suggestion, any mean deformations fall in the range $-1 \leqslant \pi \leqslant 1$: $\pi = -1$ corresponds to a pure rotation, $\pi = 0$ a pure shear and $\pi = 1$ a pure strain, where $\pi = (S_{ij}S_{ij} - W_{ij}W_{ij})/(S_{ij}S_{ij} + W_{ij}W_{ij})$. The flows with a strong strain ($\pi \to 1$) have a significant history effect and turbulence models based on an eddy viscosity concept for Reynolds stresses lead to non-physical predictions in even the mean flow. An example is the k–ε model application to a strain-dominated impinging jet flow, where eddy viscosity formula with its inadequate presentation of the anisotropy of the normal stresses overpredicts the energy production terms.

As shown in Fig. 5, the deformation of flow is siginificant in the vicinity of impinging region. To avoid this erroneous behavior, a different value of C_μ should be taken or C_μ should be varied depending on flow deformations. In this region, the normal stress ($\overline{u^2} = 2k/3 - 2\nu_t S_{11}$) of the standard k–ε model represents negative values. This implies that the constant values of $C_\mu = 0.09$ are not appropriate in the eddy viscosity equation. In the present study, the $f_{\mu 2}$ function of Eq. (23) enforces the realizability for Reynolds stresses by imposing the mean strain rate variation. As seen in Fig. 6, the influence of $f_{\mu 2}$ is significant in the impinging region. The prediction with $f_{\mu 2} = 1$ is similar to the result of the k–ε model. This exemplifies a closer interrelation between the value of C_μ and the flow deformation. The present model with the realizability for irrotational strains shows a better agreement.

The predicted distributions of turbulent kinetic energy (k) and eddy viscosity (ν_t) near the stagnation region are compared in Fig. 7 for two cases, i.e., $Re_D = 23\,000$ and $Re_D = 70\,000$ at $H/D = 2$. A closer inspection of the profiles of k and ν_t reveals that $f_{\mu 2}$ prevents the excessive high turbulence

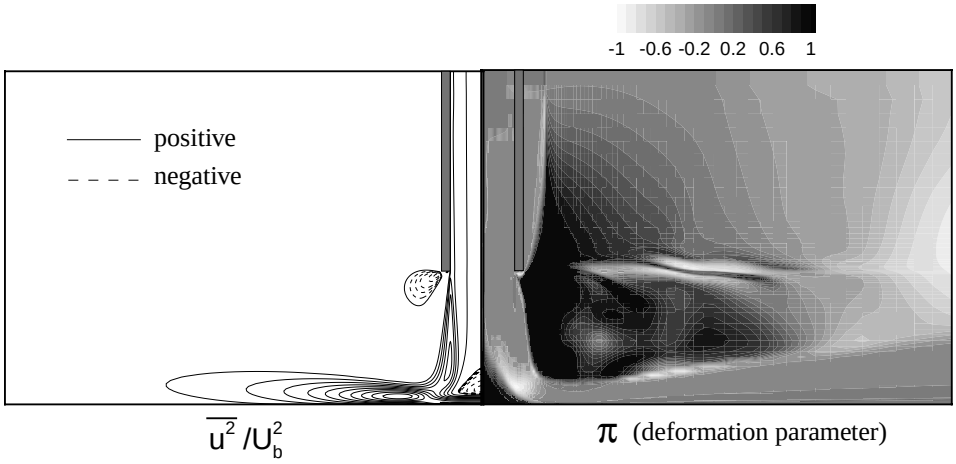

Fig. 5. Realizability of standard k–ε model.

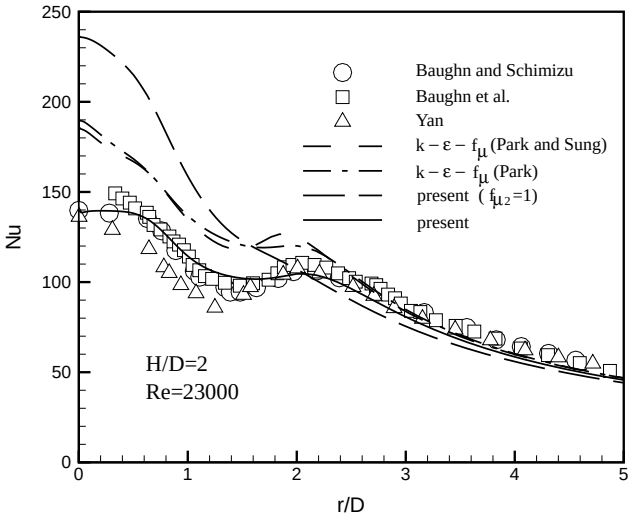

Fig. 6. Comparison of k–ε–f_μ models with experiments.

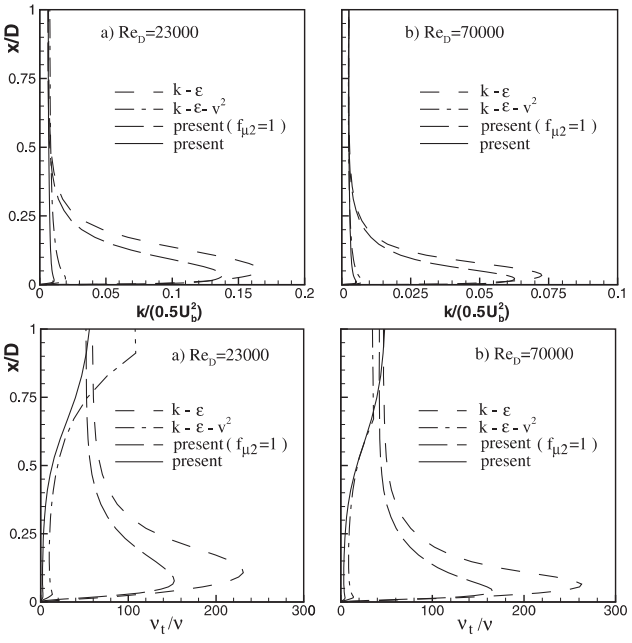

Fig. 7. Model predictions of k and ν_t.

level in the stagnation region. The k–ε model and the present model with $f_{\mu 2} = 1$ show highly diffusive results in the stagnation region, while the k–ε–v^2 model and the present model predict the realizable turbulent energy and eddy diffusion. This suggests that the present $f_{\mu 2}$ model works well in suppressing the turbulent diffusivity in the near-wall region of strongly strained turbulent flow. As Re_D increases, the peak of k in the near-wall region decreases.

Next, the profiles of normalized mean velocity are shown in Fig. 8. The predicted results by three turbulence models are compared with the experimental data of Cooper et al. (1993). Near the stagnation region, all predictions are consistent with the experiment. In the wall jet boundary layer where the flow is accelerated, the k–ε model shows an underprediction in the wall layer and an overprediction in the outer region. This deviation is attributed to the wall jet development from highly

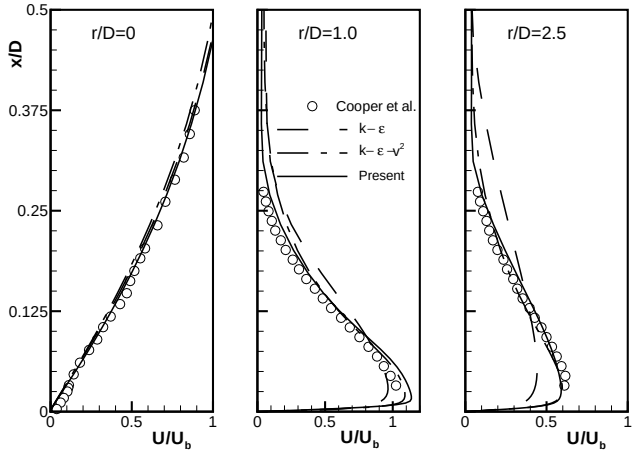

Fig. 8. Model comparisons of U/U_b with experiment ($H/D = 2$ and $Re_D = 23\,000$).

diffusive stagnation flow. However, the k–ε–f_μ and the k–ε–v^2 models resolve the behavior well, because the stresses of two models are realizable in the stagnation region.

3.3. Heat transfer

When an eddy viscosity model is used in the prediction of heat transfer, the most important factor in determining the local transport is the distribution of turbulent thermal diffusivity ($\alpha_t = \nu_t/Pr_t$). In order to evaluate the effect of Pr_t, two constant values and an empirical formula of Kays and Crawford (1993) are employed. For $H/D = 2$ and $Re = 23\,000$, the predicted results are compared with the relevant experimental data (Baughn and Shimizu, 1989; Baughn et al., 1991; Yan, 1993). As shown in Fig. 9, the results are in good agreement with the measurements. Note that the formula of Kays and Crawford (1993) gives a somewhat better agreement in the stagnation region. However, a slight underprediction is seen in the downstream ($r/D \geqslant 1.5$). In general, as Pr_t decreases, the wall heat transfer increases. A good agreement with the experiment is seen at $Pr_t = 0.9$.

The Nu distributions for $H/D = 2$ and $Re_D = 23\,000$ are represented in Fig. 10. The predicted results are compared with

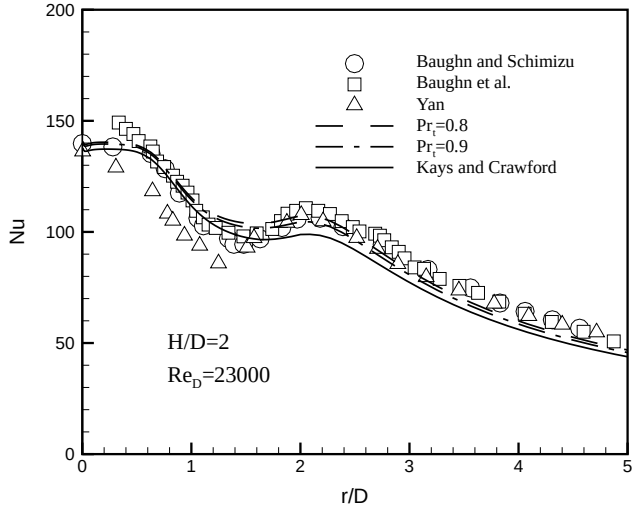

Fig. 9. Effect of Pr_t on Nu.

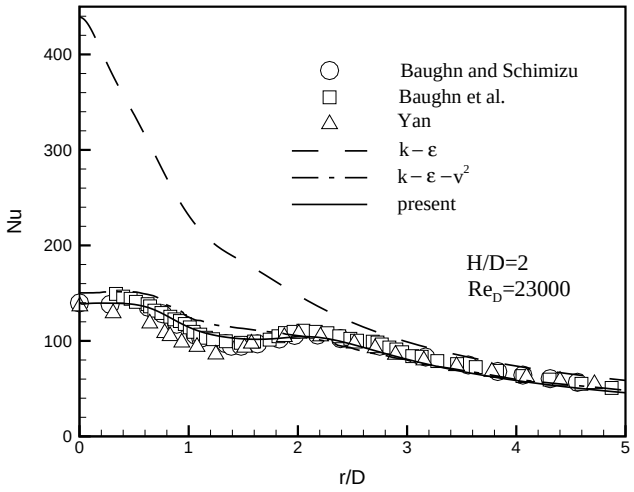

Fig. 10. Model comparisons of *Nu* with experiments.

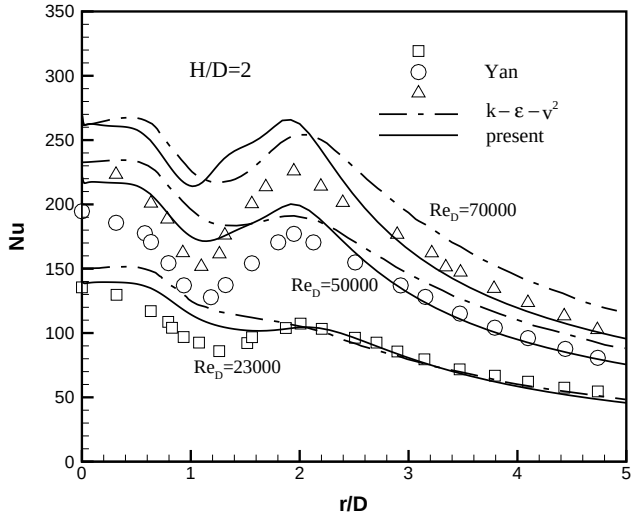

Fig. 11. Model comparisons of *Nu* with experiments at three Reynolds numbers ($Re_D = 23\,000$, 50 000 and 70 000).

the experimental data. The results by the k–ε–v^2 model are also displayed for comparison. This is based on the belief that the k–ε–v^2 model can be regarded as a reliable model for predicting the jet impingement heat transfer. As shown in Fig. 10, the present k–ε–f_μ model follows the experimental data well. It is evident that the stagnation heat transfer is significantly overpredicted by the k–ε model. The k–ε model overpredicts about 300% in the stagnation region. A closer inspection of Fig. 10 indicates that a second peak is displayed by the present k–ε–f_μ model. It is known that the second peak is associated with the maximum turbulent kinetic energy near the wall. Within the range of $r/D = 1$ to 2, the *Nu* distribution computed with the k–ε–v^2 model overpredicts slightly, while the present model gives an excellent agreement with experimental data. This region is a transition zone where the stagnation flow is transformed into a radial wall jet. The ring shaped wall eddies are induced by large scale toroidal vortices hitting the plates (Popiel and Olev, 1991). These eddies enhance local momentum and heat transfer, which are responsible for the second peak. Moreover, a second peak is clearly displayed by the present model in Fig. 10. As mentioned earlier, since the k–ε–f_μ model includes the non-local near-wall effect and the realizable eddy viscosity in strongly strained turbulent flows, an improved performance is anticipated.

The *Nu* distributions for three Reynolds numbers ($Re_D = 23\,000$, 50 000 and 70 000) are displayed in Fig. 11. These results are compared with the experimental data of Yan (1993). It is seen that some discrepancies are found between experiment and computation. However, the discrepancy diminishes downstream of the stagnation region. As Re_D increases, the edge vortex of jet flow is strengthened.

4. Conclusions

In order to make a realizable stress–strain relation, the k–ε–f_μ model has been modified with the aid of the Cayley–Hamilton theorem and the realizability constraint. The $f_{\mu 2}$ function was introduced to derive a realizable eddy viscosity. It prevented the spurious generation of turbulent kinetic energy by imposing the variations of C_μ to the mean strain rates. The effect of $f_{\mu 2}$ on *Nu* was significant in the impinging region. The near-wall effect and the anisotropic production were reflected in the ε-equation. In the first, the present model was tested for a fully developed channel flow and a separated and reattaching flow over a backward-facing step. The predicted results reproduced the wall limiting behavior successfully. The computed *Nu* showed a good agreement with the experimental data while the k–ε model overpredicted. The monotonic decrease of *Nu* was attenuated near $r/D = 2$. This behavior was due to the insensibility of eddy viscosity in strongly strained flows. The velocity magnitude profile was consistent with the measurements in the region $r/D \geqslant 1.5$. The development of radial wall jet for three Reynolds numbers was satisfactory. The dynamic and thermal characteristics of impinging jet flow were well captured by the present model.

Acknowledgements

This work was supported by a grant from the National Research Laboratory of the Ministry of Science and Technology, Korea.

References

Baughn, J., Shimizu, S., 1989. Heat transfer measurements from a surface with uniform heat flux and an impinging jet. ASME J. Heat Transfer 111, 1096–1098.

Baughn, J., Hechanova, A., Yan, X., 1991. An experimental study of entrainment effects on the heat transfer from a flat surface to a heated circular impinging jet. ASME J. Heat Transfer 113, 1023–1025.

Behnia, M., Parneix, S., Durbin, P.A., 1998. Prediction of heat transfer in an axisymmetric turbulent jet impinging on a flat plate. Int. J. Heat and Mass Transfer 41 (12), 1845–1855.

Cooper, D., Jackson, D., Launder, B., Liao, G., 1993. Impinging jet studies for turbulence model assessment-I. Flow-field experiments. Int. J. Heat Mass Transfer 36, 2675–2684.

Cotton, M.A., Ismael, J.O., 1993. Development of a two-equation turbulence model with reference to a strain parameter. In: Proceedings of the Fifth International Symposium on Refined Flow Modeling and Turbulence Measurements. Paris, pp. 117–124.

Craft, T.J., Graham, L., Launder, B.E., 1993a. Impinging jet studies for turbulence model assessment-II. An examination of the perfomance of four turbulence models. Int. J. Heat Mass Transfer 36, 2685–2697.

Craft, T.J., Launder, B.E., Suga, K., 1993b. Extending the applicability of eddy-viscosity models through the use of deformation invariants and nonlinear elements. In: Proceedings of the Fifth International Symposium on Refined Flow Modeling and Turbulence Measurements. Paris, pp. 125–132.

Craft, T.J., Launder, B.E., Suga, K., 1996. Development and application of a cubic eddy-viscosity model of turbulence. Int. J. Heat Fluid Flow 17, 108–115.

Durbin, P.A., 1993. A Reynolds-stress model for near-wall turbulence. J. Fluid Mech. 249, 465–498.

Durbin, P.A., 1996. On the k–ε stagnation anomaly. Int. J. Heat Mass Transfer 17, 89–90.

Durbin, P.A., Laurence, D., 1996. Nonlocal effects in single point closure. In: Third Advances in Turbulence Research Conference, Korea Uinversity, Korea, pp. 109–120.

Gatski, T.B., Speziale, C.G., 1993. On explicit algebraic stress models for complex turbulent flows. J. Fluid Mech. 254, 59–78.

Hunt, J.C.R., 1992. Developments in computational modeling of turbulent flows. In: Pironneau, O., Rodi, W., Ryhming, I.L., Savill, A.M., Truong, T.V. (Eds.), Numerical Simulation of Unsteady Flows and Transition to Turbulence. pp. 1–76.

Kasagi, N., Tomita, Y., Kuroda, A., 1992. Direct numerical simulation of passive scalar field in a turbulent channel flow. ASME J. Heat Transfer 114, 598–606.

Kays, W.M., Crawford, M.E., 1993. Convective Heat and Mass Transfer, third ed. McGraw-Hill, New York.

Moser, R.D., Kim, J., Mansour, N.N., 1999. Direct numerical simulation of turbulent channel flow up to $Re_\tau = 590$. Phys. Fluids 11 (4), 943–945.

Park, T.S., 1999. Multigrid method and low-Reynolds-number k–ε model for turbulent recirculating flows. Numer. Heat Transfer Part B: Fundamentals 36, 433–456.

Park, T.S., Sung, H.J., 1995. A nonlinear low-Reynolds-number k–ε model for turbulent separated and reattaching flows – (I) flow field computation. Int. J. Heat Mass Transfer 38 (14), 2657–2666.

Park, T.S., Sung, H.J., 1997. A new low-Reynolds-number k–ε–f_μ model for predictions involving multiple surfaces. Fluid Dyn. Res. 20, 97–113.

Popiel, C.O., Olev, T., 1991. Visualization of a free and impinging round jet. Exp. Therm. Fluid Sci. 4, 253–264.

Speziale, C.G., Gatski, T.B., 1997. Analysis and modelling of anisotropies in the dissipation rate of turbulence. J. Fluid Mech. 344, 155–180.

Speziale, C.G., Sarkar, S., Gatski, T.B., 1991. Modeling the pressure–strain correlation of turbulence: an invariant dynamical systems approach. J. Fluid Mech. 227, 245–272.

Tavoularis, S., Karnik, U., 1989. Further experiments on the evolution of turbulent stresses and scales in uniformly sheared turbulence. J. Fluid Mech. 204, 457–478.

Yan, X., 1993. A preheated-wall transient method using liquid crystals for the measurement of heat transfer on external surfaces and in ducts. PhD Thesis, University of California, Davis.